Lag synchrony measures dynamical processes underlying progression of seizure states

Benjamin H. Singer, Miron Derchansky, Peter L. Carlen, and Michał Żochowski
Neuroscience Program, Department of Physics and Biophysics Research Division, University of Michigan, Ann Arbor, Michigan 48109, USA
Division of Cellular and Molecular Biology, Toronto Western Research Institute, Ontario, Toronto, Canada M5T 2S8
(Received 10 November 2005; published 17 February 2006)

We investigate the dynamics of bursting behavior in an intact hippocampal preparation using causal entropy, an adaptive measure of lag synchrony. This analysis, together with a heuristic model of coupled bursting networks, separates experimentally observed bursting dynamics into two dynamical regimes, when bursting is driven by (1) the intranetwork dynamics of a single region, or (2) internetwork feedback between spatially disjoint neural populations. Our results suggest that the abrupt transition between these two states heralds the gradual desynchronization of bursting activity. These results illustrate how superficially homogeneous behavior across loosely coupled networks may harbor hidden, but robust, dynamical processes.

DOI: 10.1103/PhysRevE.73.021910 PACS number(s): 87.18.Hf, 87.18.Sn, 05.45.Xt

INTRODUCTION

Synchrony is observed in a wide range of physical and natural systems. It is thought to play an important role during information processing in the brain and at the same time underlies one of its major dynamical diseases—epilepsy. One of the more important issues in study of synchrony is the deduction of the causal relationships between synchronized events, in order to characterize the dynamics of spatially distributed systems. To achieve that goal, multiple methods have been constructed based on phase space reconstruction [1], state space properties [2–5], information transfer [6,7], measurement of phase differences [8–12], or the notion of event synchronization [13]. Many studies have used these methods in investigations of seizure onset with the goal of seizure prediction [14–16]. Although both linear and nonlinear techniques have been employed to study seizure localization and propagation, fewer studies have examined the dynamics of seizure progression [17–24].

Here we use the notion of lag stability during phase or lag synchronization [25–27] to investigate the progression of bursting dynamics observed in the intact *ex vivo* hippocampus. We monitor evolution and stability of the lags between the bursting events recorded at four different sites in the hippocampus, using a measure that we have previously developed. We show that the driving pattern (monitored by the time lag measurement between the bursts) between the different hippocampal regions evolves during the bursting dynamics. Initial stability of the leading region in the septal hippocampus evolves into switching of the burst lead location.

Furthermore, we show that the relative internal dynamical properties of the recorded locations do not simply follow the lead pattern. Initially, bursting at the site that exhibits the highest degree of synchrony leads the bursting at other regions. However, in time this pattern changes dramatically and the regions with a lesser degree of synchrony lead the bursting dynamics. To better understand this dramatic change we study the dynamics of a heuristic model of two interconnected networks composed of integrate and fire neurons. We show that this model captures the basic dynamical features observed experimentally and allows us to explain the lead switching taking place in the hippocampus. Our simulation results indicate that the lead switching heralds the end of bursting dynamics in the network as the slow dissolution of the seizure commences.

I. MULTISITE RECORDINGS OF BURSTING ACTIVITY

Hippocampi of C57/BL6 mice (P8-P25) were isolated in accordance with Canadian Animal Care Guidelines and perfused with low-Mg^{2+} artificial cerebrospinal fluid (ACSF) to induce bursting activity [28]. Local field potential recordings were made from the CA1 layer of the hippocampus with a four-channel multiple electrode array with an interelectrode distance of 300 μm and an interpair distance of 1500 μm [Fig. 1(a)]. Data were acquired using an eight-pole Bessel low-pass filter (700 Hz) and digitized at 2 kHz. The resulting recordings display intermittent episodes of sustained bursting [seizure-like events (SLEs)], with coincident bursts recorded on all four electrodes. A single SLE recorded at four sites is illustrated in Fig. 1(b). To extract interburst interval information from recordings of hippocampal local field potential, burst event times are isolated from the recording by low-pass filtering at 10 Hz with a digital eight-pole Bessel filter, followed by thresholding at 5% of the maximum deviation above the mean [Fig. 2(b)].

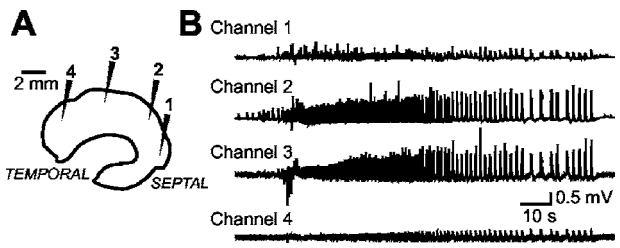

FIG. 1. (a) Schematic of the explanted mouse hippocampus showing the approximate placement of electrodes. (b) Representative local field potential recording of a single SLE from four positions in the hippocampus.

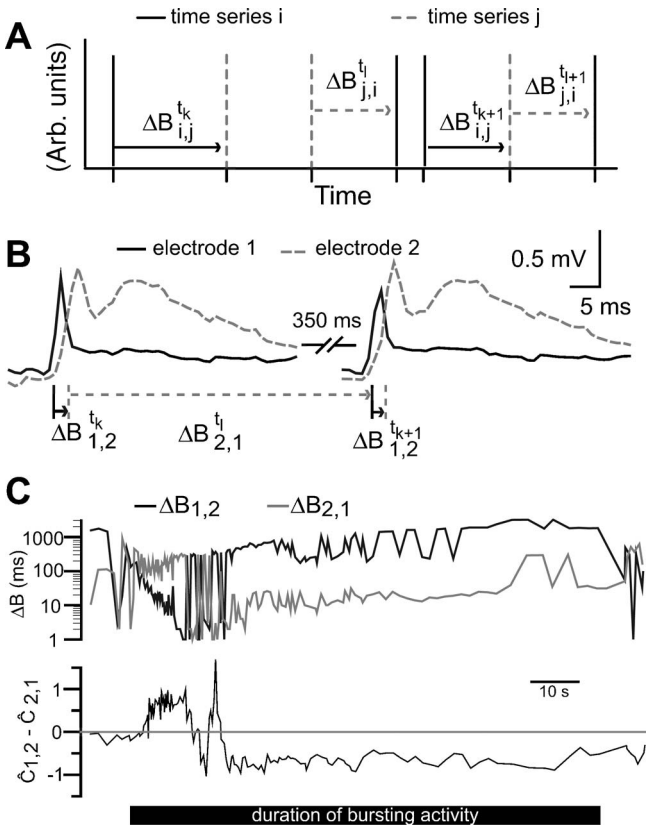

FIG. 2. (a) General schema for calculating interburst intervals (ΔB) from two electrodes. (b) Expanded view of two consecutive bursts recorded from two adjacent electrodes in the hippocampus, demonstrating the calculation of ΔB from the data. (c) Upper panel: Representative record of $\Delta B^t_{1,2}$ and $\Delta B^t_{2,1}$ over the course of a single SLE. Lower panel: Record of $\hat{C}_{1,2}-\hat{C}_{2,1}$ (arb. units) calculated from the ΔB time series above.

II. DIRECTIONAL RELATIONSHIPS AND LAG SYNCHRONY

To discern the dynamic relationship among the four recorded neural populations, we use a modified version of a measure we have previously developed to assess temporal interdependencies between two [29] or more [30] coupled nonidentical dynamical units. The measure continuously monitors the changes in the relative interburst intervals (ΔB) between electrode pairs. The intervals are calculated separately among events recorded on every electrode pair (i,j) in the network and among all events recorded on a single electrode.

In general, the interval $\Delta B_{i,j}$ of the time series i with respect to the time series j is calculated as the time difference between an event in j and the immediately preceding event in i. The value of this interval is then assigned the time stamp of the event in i. The interval $\Delta B_{j,i}$ of j with respect to i is calculated similarly, with the value of each interval assigned to the time stamps of events in j. The intervals $\Delta B_{i,i}$ are calculated as the time difference between each sequential event appearing on the ith electrode. Events are evaluated sequentially in time. The time at which the originating event of each interburst interval occurs is recorded, forming the time series $\Delta B^t_{i,j}$ for each (i,j) [Fig. 2(a)]. The asymmetric relationship among two event series may be monitored by studying the relative properties of $\Delta B^t_{i,j}$ and $\Delta B^t_{j,i}$. If the signal i drives the signal j, then the events of j are likely to follow those of i with a nearly constant lag, and the values of $\Delta B^t_{i,j}$ will be tightly clustered. Conversely, if the signal j has little driving influence over i, then the values of $\Delta B^t_{j,i}$ will be widely distributed.

The difficulties of detecting true driving within coupled, nonidentical dynamical systems have been discussed extensively in Ref. [4]. In the study of recordings from neural systems, it is possible that apparent driving relationships are due to true driving by an unmeasured source. However, the apparent driving relationships between two or more time series may still have utility insofar as they contain information regarding the properties of the unmeasured, true source of activity. Here, to avoid confusion, we will replace the notion of "driving" with "leading" to reflect the limitations of our observations.

The occurrence of asymmetric interburst interval distributions in the neuronal bursts is illustrated in Fig. 2(b) on a burst-to-burst basis. While the bursts recorded on each electrode are highly coincident, there is a temporal lag in the activity recorded by different electrodes. Therefore, the values of $\Delta B^t_{1,2}$ are on the order of 3–5 ms and display little variability, while the values of $\Delta B^t_{2,1}$ are over 350 ms, and display high variability among bursts. Similar calculations of $\Delta B^t_{i,j}$ are performed for $(i,j)\in\{(1,2),(2,3),(3,4)\}$.

The asymmetry in $\Delta B^t_{i,j}$ and $\Delta B^t_{j,i}$ distributions changes over time, as illustrated in Fig. 2(c) (upper trace). As recurrent bursting activity commences (black bar), $\Delta B^t_{1,2}$ is small and has low variance, while $\Delta B^t_{2,1}$ is larger and has higher variance, indicating that the bursts recorded on channel 2 lag those recorded on channel 1. Conversely, after a period of rapid variation the values of $\Delta B^t_{2,1}$ are small and have low variance, while the values of $\Delta B^t_{1,2}$ are large and have high variance, indicating that the bursts recorded on channel 1 lag those recorded on channel 2.

In order to quantify the distribution of $\Delta B^t_{i,j}$ through time, we create a histogram with bins I_l of equal width ΔT spanning the values of the ΔB time series for each (i,j). This histogram is updated continuously at the time when new events occur on the electrodes i and j. Specifically, if a new ΔB is generated such that $l\Delta T<\Delta B^{t_k}_{i,j}\leqslant(l+1)\Delta T$, then the bin I_l at the time t_k will be updated so that $I^{t_k}_l=I^{t_{k-1}}_l+\Delta P$. All bins I are then renormalized to a total weight of unity. Thus, ΔT controls the sensitivity of the distribution to small differences in interburst interval (IBI), and ΔP controls the degree to which the interburst interval distribution takes into account early, as opposed to recent, events in the ΔB time series [29].

After each such update, the Shannon entropy $S=-\Sigma_l I_l \ln I_l$, of the renormalized IBI distribution is calculated. We refer to it as a causal entropy of electrode i vs electrode j at time t_k ($C^{t_k}_{i,j}$). For simplicity of notation we will suppress the time index, with the understanding that $C_{i,j}$ refers to the value of the causal entropy at a specific time.

Since the relative interburst intervals are measured unidirectionally [Figs. 2(a) and 2(b)], the pairwise comparison of

$C_{i,j}$ and $C_{j,i}$ through time allows the asymmetric measurement of temporal interdependencies between the activity at two electrodes. To account for the possibility that the temporal interdependence between two signals could be an artifact of autonomous temporal signal properties (e.g., frequency) on one (or both) electrodes we calculate the quantity

$$\hat{C}_{i,j} = \frac{\min(C_{i,i}, C_{j,j}) - C_{i,j}}{\min(C_{i,i}, C_{j,j})}, \quad (1)$$

where $C_{i,i}$ is the entropy of (continuously updated) interburst interval distributions observed on a single electrode ($\Delta B_{i,i}$). Values of $\hat{C}$ around and below zero indicate that there is no significant interdependence between the signals, whereas if $\hat{C}$ tends to unity this indicates strong temporal interdependence. This measure detects and categorizes three basic regimes: the lag-synchronous state is not achieved—the two electrodes are independent (both $\hat{C}_{i,j}$ and $\hat{C}_{j,i} \to 0$); lag synchrony is observed and electrode i leads electrode j ($\hat{C}_{i,j} \gg 0$ while $\hat{C}_{j,i} \to 0$); and the equivalent state where j leads i; the signal is nearly periodic or is completely synchronized (both $\hat{C}_{i,j}$ and $\hat{C}_{j,i} \gg 0$).

Changes in the relative values of $\hat{C}_{i,j}$ and $\hat{C}_{j,i}$ are most easily visualized by the difference between these two quantities. $\hat{C}_{i,j} > \hat{C}_{j,i}$ indicates that $\Delta B_{i,j}$ is less variable than $\Delta B_{j,i}$, and therefore that activity in j is causaly related and systematically lags after activity in i. For example, the time series of $\hat{C}_{1,2} - \hat{C}_{2,1}$ in Fig. 2(c) (lower trace) quantifies the trends in $\Delta B_{1,2}$ and $\Delta B_{2,1}$ observed above. The activity in channel 1 initially leads that in channel 2, followed by a brief period of lead switching, following which the activity in channel 2 stably leads the activity in channel 1.

In order to determine the significance of observed $\hat{C}$ values, we compute surrogate data sets by randomly reassigning event times from each electrode to new electrode labels (shuffled data set). ΔB and $\hat{C}$ values are then computed from these shuffled data sets. This procedure preserves the overall frequency characteristics of the signals over time, while destroying the fine, directional temporal relationships between events recorded at each electrode. Thus, the distribution of $\hat{C}$ values computed from shuffled data sets reflects the null hypothesis that all four signals are autonomous, but possess similar characteristics in the frequency or time domain. Thresholds for significance are then based on the distribution of $(\hat{C}_{j,i} + \hat{C}_{i,j})$ and $(\hat{C}_{j,i} - \hat{C}_{i,j})$ over ten shuffled data sets (Fig. 3).

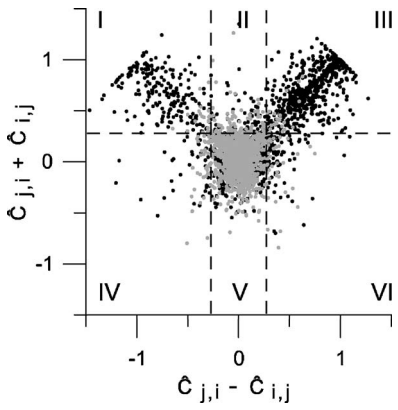

FIG. 3. Two-dimensional plot of $\hat{C}_{j,i} + \hat{C}_{i,j}$ vs $\hat{C}_{j,i} - \hat{C}_{i,j}$ (arb. units) for a representative SLE (black). Values of $\hat{C}_{i,j}$ are paired with their nearest temporal neighbors in $\hat{C}_{j,i}$. Thresholds for $\hat{C}$ sum and difference are set based on the distributions obtained from surrogate data sets (gray). Thresholds are set at the 95th percentile of $\hat{C}_{j,i} + \hat{C}_{i,j}$ (horizontal line), and the 2.5th and 97.5th percentiles of $\hat{C}_{j,i} - \hat{C}_{i,j}$ (vertical lines). The intersections of these thresholds form six sectors. In sector I, activity in i significantly leads activity in j, while in sector III, activity in j significantly leads activity in i. Events in other sectors are not significant.

A. SLEs display a stereotyped pattern of lag synchrony

Events that fall outside the significance threshold for both $\hat{C}$ sum and difference for each of the electrode pairs $(i,j) \in \{(1,2),(2,3),(3,4)\}$ are depicted in a raster plot of individual events and lag pattern [Fig. 4(a)]. We found well-defined temporal regions during every SLE when the pattern of lag synchrony between electrodes is stable. Furthermore, as illustrated within the depicted SLE, the septal (electrode 1) region of the hippocampus initially leads all other regions [Fig. 4(a), region *a*]. After the initial period of leading by the septal electrode, the lead patterns switch and only intermittent lag synchrony is achieved for the remaining duration of the SLE [Fig. 4(a), region *b*]. We refer to this epoch of the SLE as the period of directional switching. These two periods (septal leading and directional switching) are observed in each of 15 SLEs recorded from six hippocampi [Fig. 4(b)]. The duration of septal leading is 23.1 ± 13.9 s, while the duration of directional switching is 73.3 ± 78.3 s per SLE.

III. PROPAGATION OF BURSTING IN COUPLED NETWORKS OF INTEGRATE AND FIRE NEURONS

Our analysis of SLE recordings in the intact hippocampus suggests that the recurrent bursting is divided into two distinct periods: septal leading and directional switching. Both periods are characterized by lag synchrony of two distinct, but coupled, neural populations. However, this temporal variation in lag synchrony does not illuminate the underlying changes in neural population dynamics throughout the SLE.

In order to further elucidate the dynamical mechanisms underlying the observed temporal patterns, we build a heuristic computational model capturing basic properties of the experimental system. We assume that each region recorded by a single electrode constitutes a local network [31–33]. While hippocampal networks possess intricate patterns of connectivity and many types of inhibitory interneurons essential for information processing, here we are interested in the gross features of bursting events and the importance of broad measures of excitability to the origin and propagation of bursting activity among local networks. The model is not intended to capture details of the neurobiology underlying SLE generation.

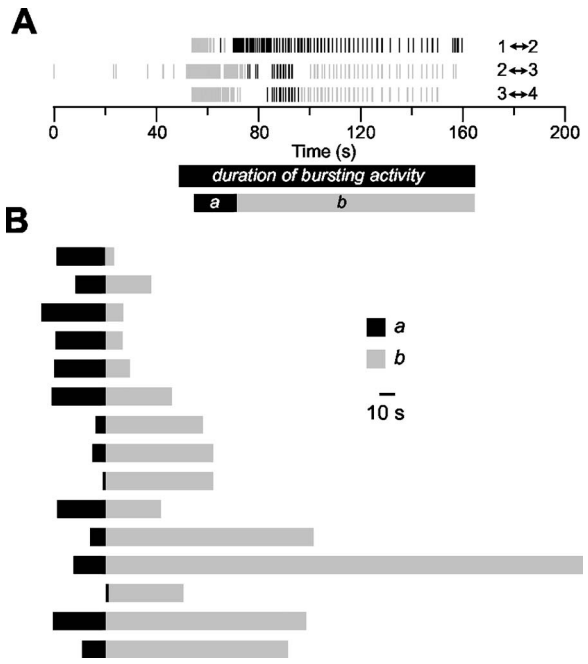

FIG. 4. (a) Raster plots for a representative SLE showing times of events pairs among adjacent electrodes $(i,j) \in \{(1,2),(2,3),(3,4)\}$ with significant $\hat{C}$ sum and difference values; gray, septal electrode leads temporal; black, temporal electrode leads septal. Electrode 1 is most septal, while electrode 4 is in the most temporal position. The overall pattern of leading begins as septal→temporal (area *a*) and then enters an epoch of directional switching (area *b*). (b) Relative lengths of septal→temporal phase (area *a*) and postswitching phase (area *b*) in 15 SLEs recorded from six hippocampi. Bars are aligned to the first directional switch. Mean(standard deviation) duration of $a=23.1$ (13.9) s, $b=73.3$ (78.3) s.

Therefore, our model includes only excitatory neural oscillators and a generalized connectivity pattern. We create two interconnected networks (designated *N*1 and *N*2) of integrate and fire neurons with a small world network (SWN) architecture, with each neuron positioned on a two-dimensional 15×15 lattice with periodic boundary conditions and uniform spacing between nodes. The SWN architecture [34] has been reported in neural structures, and has been linked to seizure generation [35].

SWN structure in each network is obtained by first connecting all neighbors in the lattice, and then randomly removing or adding connections within a radius $k=2$ with a rewiring probability of $p=0.3$ for each connection. This results in a network having an overall connectivity ratio of 0.05. Additionally, a randomly selected fraction ($f=0.3$) of neurons in each network receives synaptic input from a randomly chosen group of $m=10$ neurons from the other network. The dynamics of each neuron are given by:

$$\frac{dV_i}{dt} = -\alpha_i V(t) + A\sum_{j\in C} J_{i,j}(t) + B\sum_{k\in I} J_{i,k}(t) + \xi(t) \qquad (2)$$

where $A=4$ determines the intranetwork signal amplitude, $B=0.4$ is the internetwork signal amplitude, $\alpha_i \in (1.0,1.5)$ is the membrane leakage coefficient (different for every neuron in the network), and $\xi \in (1.0,1.4)$ is a random variable simulating white noise. *C* denotes the set of all neurons connected to *i*th neuron via intranetwork connections, while *I* denotes the neurons connected via internetwork connections. $J_{i,j}$ is the term describing synaptic current arriving from the *j*th neuron:

$$J_{i,j} = \exp\left(-\frac{t_s}{\tau_s}\right) - \exp\left(-\frac{t_s}{\tau_f}\right) \qquad (3)$$

where t_s is the time from the last spike generated at the *j*th neuron; $\tau_s=0.3$ ms and $\tau_f=0.03$ ms are time constants.

When the threshold $\Gamma_{spike}=1$ is reached, a spike is generated and the membrane potential is reset to 0. During a built-in postspike refractory period $T=10$ ms, the membrane does not potentiate in response to incoming stimuli. Every neuron in both networks has an additional inhibitory mechanism that resets the incoming synaptic current to zero if it is below a threshold level (Γ_{cut}). Inclusion of this threshold imposes a requirement for coincident input in spike generation. Therefore, when the value of Γ_{cut} is high, the network is relatively quiescent unless it receives coincident input to many neurons. This parameter effectively controls the onset of the bursting regime in the network. When Γ_{cut} is high the network activity is asynchronous (no bursting). Conversely, when Γ_{cut} is low in a given network, the network enters a regime of spontaneous bursting activity.

We use this model to study how the relative excitability of *N*1 and *N*2 influence the spread of bursting activity between the two networks. The parameters of the model (p, A, B, ξ) are set so that both networks are just outside a spontaneous bursting regime, and entry into this regime is controlled by Γ_{cut}. At $t=1$ s [Fig. 5(a), bottom] Γ_{cut} is set to zero in *N*1, shifting *N*1 into spontaneous bursting. The change in $\Gamma_{cut,N1}$ is a phenomenological model of a transiently lowered firing threshold, which could be due to multiple neurobiological mechanisms.

Bursting in *N*1 is generated when sufficient numbers of neurons spike simultaneously, generating a cascade effect. Thus bursting in *N*1 is initially generated through intranetwork dynamics following a delay after lowering $\Gamma_{cut,N1}$. The activity in *N*1, in turn, provides input to *N*2, resulting in bursting activity in both networks. Bursting in *N*2 is therefore a result of synchronous, internetwork signaling, the pattern of which is dictated by the internal dynamics of *N*1. In this phase of the model seizure, when $\Gamma_{cut,N1}$ is low, the bursts of *N*1 lead those of *N*2 [Fig. 5(a), black bar]. *N*1 bursts are also generally higher and narrower than *N*2 bursts, indicating greater internal synchrony of *N*1.

At $t=6$ s $\Gamma_{cut,N1}$ is reset to its original value. As a result, the dynamics of the two-network system change dramatically. Bursting activity is no longer autonomously generated by an increased intrinsic excitability of neurons in *N*1. Rather, it is transiently sustained by synaptic input from residual bursting generated during the epoch of $\Gamma_{cut,N1}=0$. Thus, the bursting dynamics of both networks are not predominantly mediated by the internal dynamics of *N*1, but by internetwork feedback. In this phase, switching in temporal

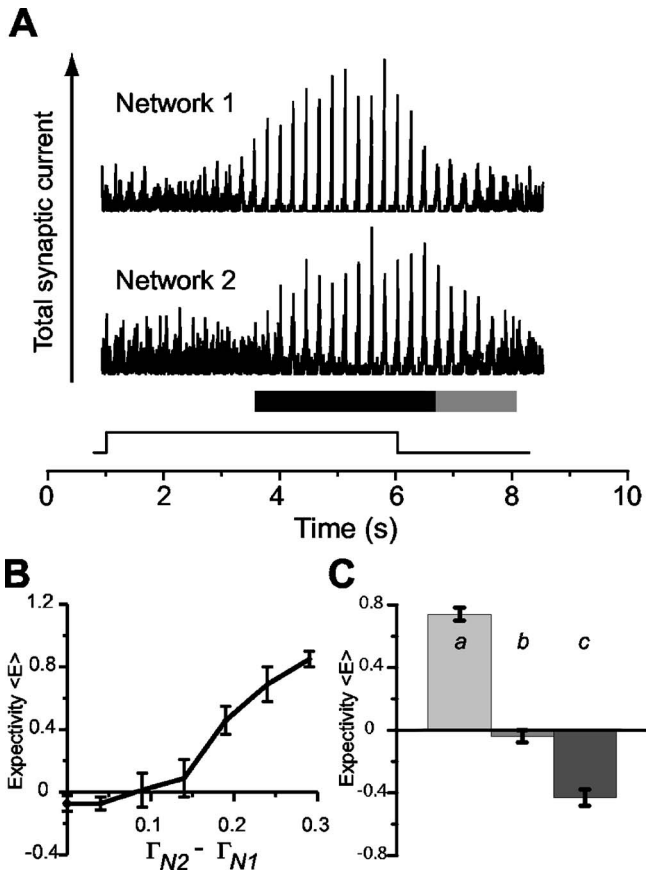

FIG. 5. (a) Total synaptic activity from each network (arb. units). In the first phase of the model seizure, activity in $N1$ leads activity in $N2$ (black bar). In the second phase, switching occurs and activity in $N2$ leads activity in $N1$ (gray bar). Step function denotes the period ($t \in [1,6]$) when $\Gamma_{cut,N1}=0$. $\Gamma_{cut,N2}=0.34$ throughout. (b) Average expectivity (arb. units) as a function of the difference in bursting thresholds in $N1$ and $N2$. $\Gamma_{cut,N1}=0.05$, while $\Gamma_{cut,N2}$ varies in [0.05, 0.29]. (c) Expectivity distinguishes three separate dynamical regimes, all of which display lag synchrony. Regime *a*: Bursting thresholds of $N1$ and $N2$ are unequal, $N1$ drives $N2$, and expectivity is positive ($\Gamma_{cut,N1}=0.05$, $\Gamma_{cut,N2}=0.29$). Regime *b*: Bursting thresholds of $N1$ and $N2$ are equal, $N1$ and $N2$ undergo sustained bursting with lead switching, and expectivity is zero ($\Gamma_{cut,N1}=0.05$, $\Gamma_{cut,N2}=0.05$). Regime *c*: Bursting thresholds of $N1$ and $N2$ are equal, $N1$ and $N2$ display diminishing bursting with lead switching, and expectivity is negative ($\Gamma_{cut,N1}=0.34$, $\Gamma_{cut,N2}=0.34$).

leading and internal synchrony is observed among the two networks [Fig. 5(a), gray bar]. Moreover, the instantaneous rate of bursting in each network is inversely linked to the size and coherence of the bursts generated by the other, consistent with bursting sustained by internetwork interactions. For example, a low-amplitude, diffuse burst in $N1$ will result in weak activation of $N2$. This, in turn, leads to decreased instantaneous frequency and gradual desynchronization of $N2$. Due to the slowing of $N2$ bursts, $N1$ activity will temporally lead bursting in $N2$—the less synchronous and smaller bursts of one network will lead the more synchronous bursts of the other until bursting ceases. Thus effectively we observe that the network that has lower instantaneous internal synchrony of the burst leads that with higher instantaneous frequency.

IV. DISTINGUISHING DYNAMIC STATES WITHIN LAG SYNCHRONY

To quantify the above effect, we define γ_{lead} as the duration of an individual burst in the temporally leading network, and γ_{lag} as the duration of the coincident burst in the temporally lagging network. Small values of γ correspond to higher degrees of internal synchrony in an individual network, as the neurons discharge within a shorter time window. The *expectivity* (E) of a burst is then defined as $+1$ if $\gamma_{lead} \leqslant \gamma_{lag}$, and -1 if $\gamma_{lead} > \gamma_{lag}$. That is, $E=+1$ when the network with greater internal synchrony leads the network with less internal synchrony, and $E=-1$ if the opposite is true. We thus link the relative properties of internal network dynamics with the driving pattern between the two networks. We have previously shown that an analogously defined measure of E in a network of Hindmarsh-Rose neurons detects transitions in the ordering of the network [30].

To evaluate how E measures asymmetries in the excitability of $N1$ and $N2$, we vary $\Gamma_{cut,N2}$ while holding $\Gamma_{cut,N1}=0.05$ constant [Fig. 5(b)]. For each pair ($\Gamma_{cut,N1}, \Gamma_{cut,N2}$), the model is integrated over 750 s. E is calculated for each coincident burst in the two networks, and the temporal average $\langle E \rangle$ calculated over the duration of the simulation. This is repeated for ten different realizations of the randomized SWN architecture described above.

When $\Gamma_{cut,N2}-\Gamma_{cut,N1}$ is small, both $N1$ and $N2$ are intrinsically excitable. Each network displays narrow bursts, and each has an equal propensity to drive the other, leading to large variations in E on a burst-to-burst basis [average $E \approx 0$, Figs. 5(b) and 5(c) regime *b*]. As $N2$ is made less excitable, the narrow, synchronous bursts of $N1$ begin to drive bursting activity in $N2$ [average $E>0$, Figs. 5(b) and 5(c) regime *a*].

In both cases above, at least one of the networks has an intrinsic tendency to generate bursting activity. To study the case in which neither $N1$ nor $N2$ possesses intranetwork dynamics leading to bursting activity, we first induce bursting by transiently setting $\Gamma_{cut,N1}=0.05$ until bursting activity is established in both networks. We then set $\Gamma_{cut,N1}$ and $\Gamma_{cut,N2}$ such that both $N1$ and $N2$ are outside the spontaneous bursting regime. E is then calculated for the bursts that occur after this point until the disappearance of high-amplitude bursts. In this case, gradually diminishing bursting activity in both networks is due to the synaptic transmission of residual bursts, not the intrinsic generation of bursts in $N1$ or $N2$ [average $E<0$, Fig. 5(c) regime *c*].

The expectivity (E) thus discriminates three different regimes of bursting activity: driving of $N2$ by $N1$, competition between the two networks, and decay of bursting dynamics. The driving regime is characterized by no lead switching events and $E>0$, competition is characterized by rapid switching and $E \approx 0$, while the bursting decay is also characterized by rapid switching but $E<0$.

In order to assess changes in the dynamical regime of a bursting activity over time, E is calculated over multiple re-

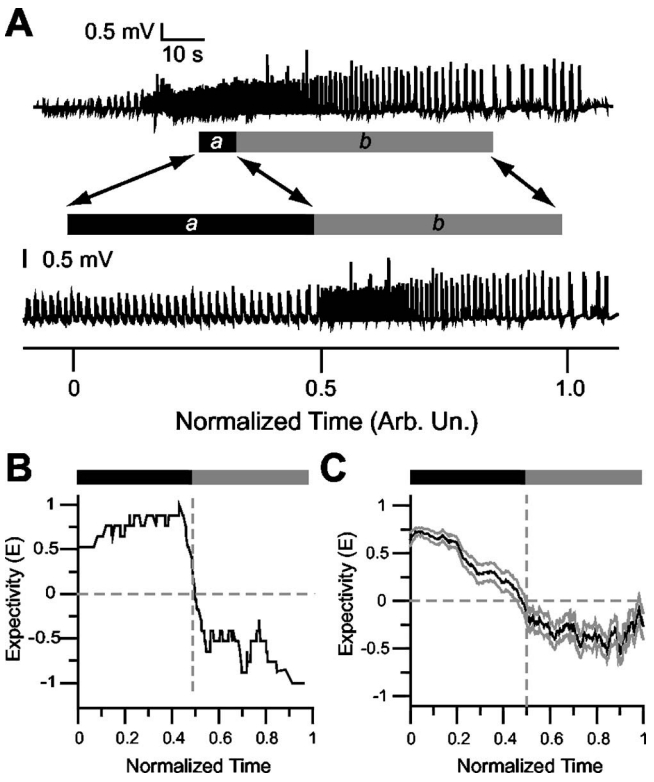

FIG. 6. (a) Illustration of time normalization procedure. (b) Average of expectivity (arb. units) among ten model seizures. Left of dashed vertical line: $\Gamma_{cut}=0.0$. Time from bursting onset to directional switching is normalized to [0, 0.5], and time from switching to end of bursting is normalized to [0.5, 1.0]. Vertical line: onset of switching. (c) Average (black)±SEM (gray) of expectivity (arb. units) among 45 electrode pairs [15 SLEs, $(i,j) \in \{(1,2),(2,3),(3,4)\}$]. Time from SLE onset to switching is normalized to [0, 0.5], and time from switching to SLE end is normalized to [0.5, 1.0]. Vertical line: onset of switching.

alizations of the two-network system described above. As shown in Fig. 4(b) the duration of bursting activity both before and after the onset of directional switching varies widely among experimentally recorded SLEs. Modeled networks also display bursting of variable duration after $\Gamma_{cut,N1}$ is restored [Fig. 5(a)]. In order to facilitate comparison of the dynamics of multiple experimental SLEs, each recording is mapped to a normalized time basis. For both model and recorded SLEs, the epoch from the onset of lag-synchronous activity to the onset of directional switching is mapped linearly to the interval $t \in [0,0.5]$ [Fig. 6(a) regime *a*], while the epoch from the onset of directional switching to the end of bursting activity is mapped to $t \in [0.5,1.0]$ [Fig. 6(a) regime *b*]. Values of E calculated on a burst-by-burst basis are then linearly interpolated through time and averaged over multiple SLEs.

A. Intra- and internetwork dynamics distinguish SLE states

In ten independent model realizations of the bursting dynamics of the type shown in Fig. 5(a), changes in average E through time conform to changes in $\Gamma_{cut,N1}$. In the first period of the model SLE, $N1$ drives $N2$ and E is positive [Fig. 6(b) left]. When $\Gamma_{cut,N1}$ and $\Gamma_{cut,N2}$ are both high, the model SLE enters a period of gradual dissolution of bursting, and E is negative [Fig. 6(b) right]. This finding is consistent with the transition from driving by intranetwork dynamics to bursting sustained by internetwork feedback.

A similar analysis is performed for 45 comparisons of activity in adjacent electrodes [15 SLEs, $(i,j) \in \{(1,2),(2,3),(3,4)\}$]. We observe that during the period of septal leading ($t<0.5$), $E>0$, as the electrode displaying narrower bursts leads the pair [Fig. 6(c) left]. After the onset of directional switching ($t>0.5$), $E<0$, with wider bursts leading [Fig. 6(b) right]. Thus, these findings support the existence of a transition from the intranetwork dynamics of a single region driving activity throughout the hippocampus to bursting sustained by internetwork feedback, leading eventually to dissolution of bursting dynamics, as observed in our model.

CONCLUSIONS

In summary, we have employed an adaptive measure of lag synchrony (causal entropy C) to identify asymmetrical patterns of lag synchrony in coincident bursting activity. We apply the measure to characterize evolution of SLE activity among four regions along the temporal-septal axis of the hippocampus. We show that after the onset of coincident activity across the hippocampus, activity measured in the septal hippocampus leads the remainder of the hippocampus. After a variable-duration period of septal leading, the lead pattern switches to leading by a nonseptal electrode. We define the onset of directional switching as the demarcation between two periods of the SLE.

Multiple groups have applied measures of nonlinear interdependence to neural time series data recorded either from models of epileptiform activity or epileptic patients [15,23]. In contrast to methods which examine synchrony in neural systems via the interdependence of analytic phases [8] or state vector representations of two time series [3,23], we examine two series of discrete events. This method is somewhat similar to event synchronization, as presented in Ref. [13], in which the authors examine depth electrode recordings from the hippocampus of an epileptic patient and also report the occurrence of a directional switch during seizure activity. Here, however, we concentrate on adaptive measurement on lag stability as a indicator of lag synchrony rather than the magnitude of the delay between the signals.

To further understand the bursting regimes we use a computational model of two coupled small world networks and examine the implications of the onset of directional switching for the dynamical underpinnings of the SLE. By combining information about temporal leading (C), with information about the internal synchrony of each individual network (burst duration), we define expectivity (E). Using a computational model, we show that E discriminates at least three distinct lag-synchronous regimes in the dynamical interrelationship of two coupled networks. When bursting activity propagates from an excitable network to a network whose excitability is below a bursting threshold, $E>0$. When bursts are exchanged between two equally excitable networks, E

≈ 0. Finally, when neither network's excitability rises above the threshold for bursting, but bursts are present due to residual excitation, $E<0$.

Based on the comparison of E measured from computational and hippocampal SLEs, we suggest that the onset of directional switching marks the abrupt transition between two dynamical states of the SLE. In the septal leading period, $E>0$, indicating that SLE behavior is dictated by the intranetwork dynamics of a localized region of the hippocampus. Conversely, $E<0$, in the directional switching period, indicating that bursting behavior is sustained by internetwork feedback among distant but coupled neuronal populations, which eventually leads to desynchronization.

This analysis demonstrates that conditional entropy effectively discriminates the dynamic states of a complex neural system. Although this analysis has focused on the bursting dynamics of seizurelike events in a model of epilepsy, the measures C and E could easily be extended to relate lag-synchrony patterns with other parameters describing autonomous characteristics of two time series. The methods could therefore be applied to discrete event data in a variety of neural systems. Comparing a measure of internetwork interaction with a measure of individual network behavior produces insight into the genesis of the transition between states. These results illustrate how superficially homogeneous behavior across loosely coupled networks may harbor hidden, but robust, dynamical processes.

ACKNOWLEDGMENTS

B.H.S. and M.Z. thank Professor Eshel Ben-Jacob, Professor Leonard Sander, and Professor Jack Parent. This work was supported by a UM Research Incentives Grant, NIH Grant No. EB003583 (M.Z.) and CIHR Research Grant No. MT14447, Krembil Scientist Development Seed Fund, and Savoy Epilepsy Foundation (P.L.C). B.H.S. is supported by the UMMS Medical Scientist Training Program (NIH Grant No. T32-GM007863) and Hearing, Balance, and Chemical Senses Training Program (NIH Grant No. T32-DC00011).

[1] D. A. Smirnov and R. G. Andrzejak, Phys. Rev. E **71**, 036207 (2005).
[2] U. Feldmann and J. Bhattacharya, Int. J. Bifurcation Chaos Appl. Sci. Eng. **14**, 505 (2004).
[3] J. Arnhold, P. Grassberger, K. Lehnertz, and C. Elger, Physica D **134**, 419 (1999).
[4] R. Quian Quiroga, J. Arnhold, and P. Grassberger, Phys. Rev. E **61**, 5142 (2000).
[5] I. Baruchi, V. L. Towle, and E. Ben-Jacob, Complexity **10**, 38 (2005).
[6] T. Schreiber, Phys. Rev. Lett. **85**, 461 (2000).
[7] P. Verdes, Phys. Rev. E **72**, 026222 (2005).
[8] M. G. Rosenblum, A. S. Pikovsky, and J. Kurths, Fluct. Noise Lett. **4**, L53 (2004).
[9] M. Palus and A. Stefanovska, Phys. Rev. E **67**, 055201 (2003).
[10] J. Lachaux, E. Rodriguez, J. Martinerie, and F. Varela, Hum. Brain Mapp **8**, 194 (1999).
[11] M. Kramer, E. Edwards, M. Soltani, M. Berger, R. Knight, and A. Szeri, Phys. Rev. E **70**, 011914 (2004).
[12] Z. Liu, J. Golowasch, E. Marder, and L. Abbott, J. Neurosci. **18**, 2309 (1998).
[13] R. Q. Quiroga, T. Kreuz, and P. Grassberger, Phys. Rev. E **66**, 041904 (2002).
[14] F. Mormann, K. Lehnertz, P. David, and C. Elger, Physica D **144**, 358 (2000).
[15] F. Mormann, R. G. Andrzejak, T. Kreuz, C. Rieke, P. David, C. E. Elger, and K. Lehnertz, Phys. Rev. E **67**, 021912 (2003).
[16] F. Mormann, T. Kreuz, R. G. Andrzejak, P. David, K. Lehnertz, and C. E. Elger, Epilepsy Res. **53**, 173 (2003).
[17] G. K. Bergey and P. J. Franaszczuk, Clin. Neurophysiol. **112**, 241 (2001).
[18] P. J. Franaszczuk, G. K. Bergey, and M. J. Kaminski, Electroencephalogr. Clin. Neurophysiol. **91**, 413 (1994).
[19] P. J. Franaszczuk, G. K. Bergey, P. J. Durka, and H. M. Eisenberg, Electroencephalogr. Clin. Neurophysiol. **106**, 513 (1998).
[20] C. C. Jouny, P. J. Franaszczuk, and G. K. Bergey, Clin. Neurophysiol. **114**, 426 (2003).
[21] J. P. Pijn, D. N. Velis, M. J. van der Heyden, J. DeGoede, C. W. van Veelen, and F. H. Lopes da Silva, Brain Topogr **9**, 249 (1997).
[22] F. Wendling, F. Bartolomei, J. J. Bellanger, and P. Chauvel, Clin. Neurophysiol. **112**, 1201 (2001).
[23] R. Quian Quiroga, A. Kraskov, T. Kreuz, and P. Grassberger, Phys. Rev. E **65**, 041903 (2002).
[24] S. J. Schiff, P. So, T. Chang, R. E. Burke, and T. Sauer, Phys. Rev. E **54**, 6708 (1996).
[25] M. G. Rosenblum, A. S. Pikovsky, and J. Kurths, Phys. Rev. Lett. **78**, 4193 (1997).
[26] M. G. Rosenblum, A. S. Pikovsky, and J. Kurths, Phys. Rev. Lett. **76**, 1804 (1996).
[27] D. Pazo, A. M. Zaks, and J. Kurths, Chaos **13**, 309 (2003).
[28] M. Derchansky, E. Shahar, R. Wennberg, M. Samoilova, S. Jahromi, P. Abdelmalik, L. Zhang, and P. Carlen, Hippocampus **14**, 935 (2004).
[29] M. Żochowski and R. Dzakpasu, J. Phys. A **37**, 3823 (2004).
[30] B. Percha, R. Dzakpasu, M. Żochowski, and J. Parent, Phys. Rev. E **72**, 031909 (2005).
[31] D. Amaral and M. Witter, Neuroscience **31**, 571 (1989).
[32] P. Buckmaster, R. Yamawaki, and G. Zhang, J. Comp. Neurol. **445**, 360 (2002).
[33] T. Gloveli, T. Dugladze, H. Rotstein, R. Traub, H. Monyer, U. Heinemann, M. Whittington, and N. Kopell, Proc. Natl. Acad. Sci. U.S.A. **102**, 13295 (2005).
[34] D. J. Watts and S. H. Strogatz, Nature (London) **393**, 440 (1998).
[35] T. I. Netoff, R. Clewley, S. Arno, T. Keck, and J. A. White, J. Neurosci. **24**, 8075 (2004).